



Sustainable Recovery of Cobalt from Aqueous Solutions Using an Optimized Mesoporous Carbon

Naby Conte¹ · Eduardo Díez¹ · Brigitte Almendras¹ · José María Gómez¹ · Araceli Rodríguez¹

Received: 15 September 2022 / Accepted: 21 December 2022 / Published online: 10 January 2023
© The Author(s) 2023

Abstract

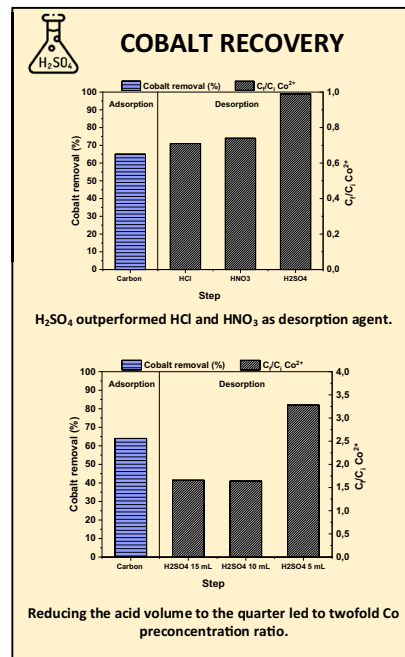
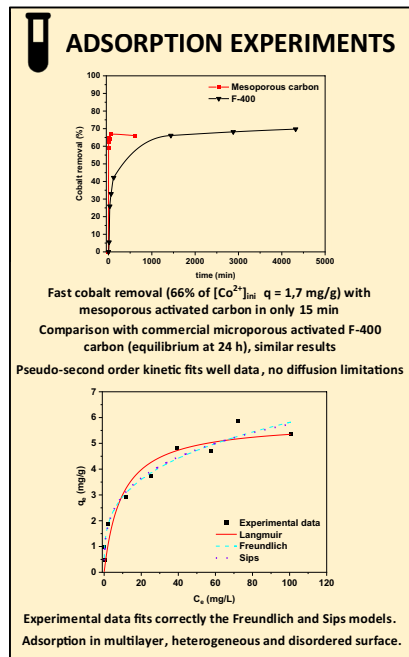
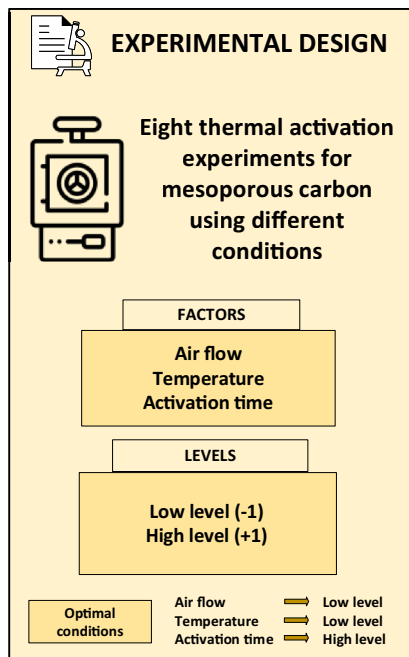
The aim of this paper is to employ a factorial design to optimize the activation step in the synthesis process of a mesoporous-activated carbon to be used as adsorbent for removing and recovering cobalt ions from aqueous solutions. This activation has been carried out in a tubular furnace in the presence of an air stream, following a 2^3 factorial design. According to the obtained results, the best activation conditions to reach a maximum cobalt removal are mild conditions, low activation temperatures and large times, while the air flow seems to be positive influence working in a low level. This is due to the enhancement of superficial oxygenated groups formation in these conditions, responsible of the adsorption process. The kinetic curve obtained for the adsorbent prepared at the most favorable conditions showed that the adsorption process was very fast and efficient, reaching equilibrium in 15 min, and was properly described by a pseudo-second-order kinetic, typical of the processes in which there are no diffusion limitations. Additionally, with the aim of studying the potential of metal recovery, desorption studies were performed. Sulfuric acid as stripping agent led to twofold Co preconcentration ratio, by reducing the desorption volume to the quarter.

The contributing editor for this article was Zhongwei Zhao.

✉ Eduardo Díez
ediezalc@ucm.es

¹ Chemical and Materials Engineering Department, Faculty of Chemistry Science, Universidad Complutense de Madrid, Madrid, Spain

Graphical Abstract



Performing the activation step using low air flows and large times improves the chemical and textural properties of the carbon. Fast adsorptive removal of 66% Co^{2+} ions is achieved with the mesoporous carbon (dosage = 10 g/L, $[\text{Co}]_{\text{ini}} = 20 \text{ mg/L}$, time = 15 min). Sulfuric acid as stripping agent succeed to perform the desorption and pre-concentration of cobalt for further uses.

Keywords Cobalt · Adsorption · Mesoporous carbon · Desorption · Factorial design

Introduction

Water pollution represents one of the most important environmental problems [1] of the present century and the future [2]. It is believed to affect future generations, the sustainable development concept and water, energy, and food production [3]. Industries such as mining operations, electronic, painting, chemical and petrochemical are the main responsible of the pollutant emissions to water. [4]. Those industries generate a huge volume of wastewater polluted with heavy metals, which are especially hazardous because of their bioaccumulation and biomagnification when the toxic ions enter the food chain and the human body afterwards [5].

Some heavy metals are regarded as strategic metals, due to their low recycling rates, limited available reserves, high risk of supply and unique properties [6]. Cobalt is one of the most important strategic metals for its applications as cathode material for manufacturing rechargeable ion-lithium

batteries for all sorts of electronic devices [7]. Therefore, as electric vehicles appear to be one of the vectors of green energy transitions with lower atmospheric emissions, in line with Sustainable Development Goal 13 (climate action), cobalt demand in the UE of 2050 is expected to be up to 15 times higher than the actual demand [8]. Currently, cobalt is obtained in the mining industry, activity that involves problems in labour rights and child labour [9]. It is imperative to explore alternative sources of this metal, i.e., the recycling from spent ion-lithium batteries [10] embracing the urban mining concept [11].

Nanofiltration, ion exchange with resins, adsorption, chemical precipitation and coagulation are technologies usually employed for the heavy metal removal [12]. Focusing on adsorption, this physicochemical technology based on mass transfer between a fluid phase and a solid surface, shines for being highly efficient for the removal of low concentrations of metals. Its simplicity, low cost-effectiveness ratio and the possibility of recovering the adsorbent by regeneration processes, make adsorption a suitable technology to remove and recover metal ions

from wastewaters [5], for further uses. In the battery metals recycling process, adsorption can be used as a technology to adjust the discharge concentrations to the permitted levels [13] or to pre-concentrate the metal for reusing.

Carbonaceous materials have been largely used as adsorbents for trapping heavy metal ions, because of their large surface area and wide porosity, thermal and mechanical stability and good adsorption performance [14]. In addition, they contain many oxygenated groups in their surface that can promote the adsorption of metallic cations [15]. Most commercially applied activated carbons possess a dominance of micropores (< 2 nm) in their internal structure, which may result in internal diffusion issues, slow kinetics, and low efficiencies at removing large compounds [16]. For that reason, research has focused in the obtention of mesoporous carbonaceous materials, with a pore range between 2 and 50 nm [17]. This allows a better accessibility of the adsorbate to the sorption sites of the carbon, improving, consequently, the adsorption kinetics and the regenerative process. It is possible to synthesize carbons with narrow and large-pore ordered structures [18] and also disordered mesoporous carbons using templates such as silica gel after being impregnated with a carbon source [14].

Heavy metal adsorption onto carbonaceous materials has been widely studied [19]. Barczak et al. studied the adsorption of some heavy metals like Pb, Zn, Cu y Cd onto an ordered mesoporous activated carbon (SBA-15 template) amino-functionalized. Large sorption capacities, were reached, with very fast kinetics [20]. Boumessaidia et co-workers investigated the adsorption of cobalt ions onto ordered mesoporous activated carbons. Cobalt removal efficiencies between 76 and 95% were achieved, reaching the equilibrium after 2 h [21]. Siddiqui et al. performed the adsorption of cobalt [22] using low-cost mesoporous carbon for the fast removal of Co^{2+} in only 6 min, removing the 95% of initial cobalt with a low dosage.

The aim of this work was to apply the factorial design technique to study and optimize the activation step in the synthesis procedure of a mesoporous activated carbon, with a suitable surface structure for a successful cobalt removal from aqueous solutions by adsorption. The influence of parameters such as air flow, temperature, and activation time were evaluated using a full factorial design for three factors, namely 2^3 design with central point replication. The activation step is crucial to obtain an activated carbon with oxygenated groups onto its surface to be used as adsorbent. It is important to point out that the main novelty of the work lies in the employment of a factorial design to optimize the synthesis of an activated carbon. Additionally, to recover the adsorbed metal ions, in pursuit of reusing the solid, desorption experiments were performed as well.

Experimental

Chemicals

Silica gel (SiO_2 , $\geq 99\%$, pore size 60 Å, particle size 40–63 μm), sucrose ($\text{C}_{12}\text{H}_{22}\text{O}_{11}$, $\geq 99.5\%$), cobalt (II) nitrate hexahydrate ($\text{Co}(\text{NO}_3)_2 \cdot 6 \text{H}_2\text{O}$ $\geq 98\%$) and hydrofluoric acid (HF, 40%) were supplied by Sigma-Aldrich. Commercial granular activated carbon F-400 was supplied by Calgon, sieved under 500 μm particle size. Sulfuric acid (H_2SO_4 , 98%) and ethanol ($\text{C}_2\text{H}_6\text{O}$, 96%), purchased by Panreac, nitric acid (HNO_3 , 69.5%), supplied by Carlo Erba and hydrochloric acid (HCl $\geq 37\%$), by Fluka were employed. Deionized water was used as well.

Mesoporous Carbons Synthesis

Disordered mesoporous activated carbon (DMC) synthesis was performed using the replica method, according to previous works [16]. After the carbonization and template elimination steps, the thermal activation was carried out in the furnace using different temperatures (400–500 °C), air flows (75–125 mL/min) and activation times (1–3 h).

Characterization

Textural characterization of the adsorbents was studied by obtaining the adsorption–desorption isotherms of N_2 at 77 K, employing a Micromeritics ASAP-2020 apparatus. Surface area and pore volume were determined using the Brunauer–Emmett–Teller (BET) equation and the single point method, respectively. To obtain the mesoporous surface (S_{meso}) and mesoporous volume (V_{meso}), the t -plot method was applied. Finally, pore size distribution curves were calculated using the Barrett–Joyner–Halenda (BJH) method. The surface chemistry and functional groups study was performed by Fourier transform infrared spectroscopy (FTIR), carried out using a Nicolet In10 MX microscope, by the Correlation Spectroscopy Research Centre of the Complutense University of Madrid.

Experimental Design

A 2^3 factorial design, where 2 stands for the number of levels, + 1 as high level and – 1 as low level, and 3 is the number of factors studied (flow, temperature, and time), was developed. This design can make considerably easier the screening of several variables with the minimum number of experiments [23]. The levels + 1 y – 1 are symmetrical about the central point, corresponding to the standard parameters employed in previous work [16]. The percentage of cobalt removed by

adsorption was selected as response variable (y). Table 1 summarizes the 2^3 factorial design. Thus, the factorial experimental design is set, with the aim of studying these variables (from now on, factors) and the interactions between them.

The 2^3 factorial design involves eight synthesis experiments, with any possible combination of the lower or higher level of each studied factor. Table 2, the design matrix, displays the geometric coding employed for each run, with their corresponding label. Apart from the eight experiments, another four runs were carried out, four activation experiments (labeled as experiment 9a, 9b, 9c and 9d) using the central point conditions. The objective of the central point replication was the determination of the experimental error during the activation process. It was established as $\pm 4\%$, as the cobalt removal with these identical carbons ranged from 68 to 72%. Once the adsorbents were synthesized, cobalt adsorption experiments were performed in duplicate ($n=2$).

Adsorption Experiments

Adsorption experiments were carried out under isotherm and batch conditions. Eppendorf tubes were used throughout the experimentation, using a TR100-G thermoblock with orbital agitation and temperature control, provided by Optic Ivymen System. To perform the experiments, a certain amount of adsorbent (activated carbon) was added to each tube, along with a volume of 2 mL of cobalt solution, prepared from the salt with the required concentration. After finishing the adsorption experiment, the liquid fraction was separated from the solid by filtration. As pH is a key parameter of the process, since cobalt can precipitate at pH values over 8 [24], this variable was controlled during the process. Metal concentration was measured by atomic absorption spectroscopy, employing a Shimadzu AA-7000 apparatus with an ASC-7000 autosampler.

Adsorption capacity (q) and the percentage of metal adsorbed were the selected criteria to evaluate the effectiveness of the adsorption. They were calculated with Eqs. (1) and (2), by mass balance.

$$q = \frac{(C_0 - C) \cdot V}{m} \quad (1)$$

$$\%Co_{adsorbed}^{2+} = \frac{(C_0 - C)}{C_0} \times 100 \quad (2)$$

Table 1 Factors and levels selected for the 2^3 factorial design

Factor	Code	Units	Low level (− 1)	Central point (0)	High level (+ 1)
Air flow	A	mL/min	75	100	125
Temperature	B	°C	400	450	500
Activation time	C	h	1	2	3

Table 2 Factors and levels selected for the 2^3 factorial design

Run	Label	Temperature		Time C
		Flow A	B	
1	1	− 1	− 1	− 1
2	a	+ 1	− 1	− 1
3	b	− 1	+ 1	− 1
4	ab	+ 1	+ 1	− 1
5	c	− 1	− 1	+ 1
6	ac	+ 1	− 1	+ 1
7	bc	− 1	+ 1	+ 1
8	abc	+ 1	+ 1	+ 1
9a	CP	0	0	0
9b	CP	0	0	0
9c	CP	0	0	0
9d	CP	0	0	0

where q (mg/g) is the adsorption capacity, or the amount of cobalt adsorbed per grams of adsorbent; C_0 y C (mg/L) relates to the cobalt concentration in the liquid phase, at zero time and at t time, respectively; V (L) is the sample volume where adsorption is carried out and m (g) is adsorbent mass.

Kinetic adsorption curves were determined by measuring the cobalt concentration in the solution at different times, and isotherm equilibrium curves were obtained similarly, preparing aliquots in the range of 5–200 mg/L and agitation until reaching equilibrium.

Cobalt desorption experiments were performed in batch using a Hettich Thermomixer MHR thermoblock. Initially, adsorption experiments were carried out in higher volume (20 mL). After reaching the equilibrium, solid and liquid phase were separated by centrifugation, and the solid part was dried and put in contact with the same volume of acid. H_2SO_4 , HCl, HNO_3 were all tested to desorb the metal. Once decided which acid had the best desorption yield, re-concentration experiments were conducted, by reducing the acid eluent volume to 15, 10 and 5 mL.

Results and Discussion

Characterization of Activated Carbons

Table 3 shows the textural properties of the activated carbons synthesized and the commercial activated carbon F-400. As it can be observed, all the synthesized materials showed large surface area, ranging between 439 and 924 m²/g. Mesoporosity is another remarkable feature, since more than 90% of their pore volume corresponded to mesopore volume. The existing differences between surface area values of the synthesized carbons are related to the activation conditions. The activation time has a positive effect on the surface area, as the highest values were obtained in experiments 5–8, in which the activation time was at its highest level (3 h). Furthermore, the activation temperature seems also have a positive effect on the surface area, since the experiments with both variables at their high level (7 and 8) led to the carbons with the largest surface area values. That behavior is examined in depth in the experimental design results. Commercial F-400 carbon shows the largest area (1117 m²/g). This is logical considering that 70% of which is micropore area, with lower pore volume. The synthesized carbon in the central point conditions showed an intermediate surface area, higher than the carbons activated for 1 h, but lower than the ones activated 3 h. Regarding the pore size distribution, Table 3 also displays the maximum diameter of each material pore size distribution, obtained with the BJH method. Despite the utilization of silica gel with pore size of 60 Å as template, the mesoporous carbons displayed a wider pore size distribution, with a maximum ranging between 90 and 130 Å. This can be attributed to the synthesis process, since thermal and mechanical treatments may cause the expansion and collapse of the small pores into larger ones. It can be observed that the average pore size is inversely proportional to the BET surface of the carbons, since the smaller the pores were, the larger the surface area would be. That is why long activation times led to a long development of the textural surface structure, with smaller pores. In any case, all the materials belong to the mesopore range (20–500 Å). On the other hand, F-400

carbon shows a maximum pore diameter at 22 Å more typical of microporous materials, being most of its pores in the micropore range.

The N₂ adsorption–desorption isotherms are shown in the Fig. 1. The shape of the isotherms of the mesoporous carbons can be associated to a type IV, according to the IUPAC [25], characteristic of mesoporous materials, with an hysteresis loop due to capillary condensation. Mesoporosity is also suggested by the increase of the quantity of N₂ adsorbed in the 0.5–0.95 relative pressure interval, which indicates a wide pore size distribution. Besides, the marked hysteresis tendency indicates the presence of mesopores wider than 4 nm. There is a marked contrast between the shape of the isotherms for the mesoporous carbons and the one obtained for the F-400 carbon. F-400 isotherm happens to be much flatter, resembling a type I isotherm, common for microporous solids [25]. This supports the 70% of microporosity according to the *t*-plot analysis.

The Fig. 2 represents the FTIR spectra of the carbonaceous materials employed. The spectra of the synthesized mesoporous carbons are very similar, showing the same absorption peaks, although with different intensity. Most of these bands are related to oxygenated surface groups,

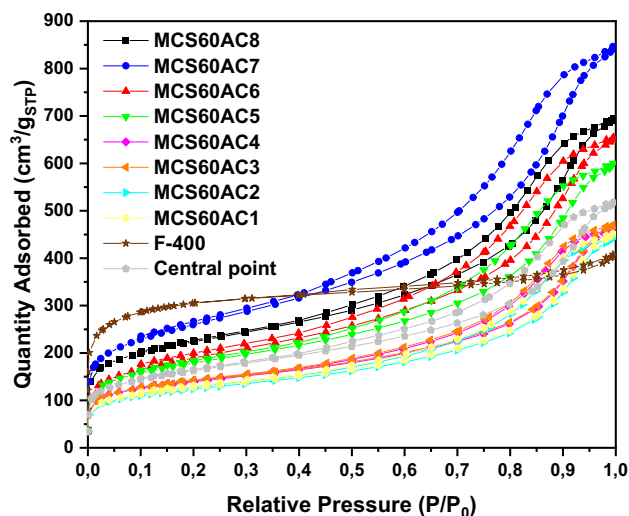


Fig. 1 N₂ adsorption–desorption isotherms at – 196 °C of activated carbons obtained at each activation experiment and commercial activated carbon F-400

Table 3 Textural characterization of activated carbons

Experiment	1	2	3	4	5	6	7	8	Central point	F-400
S_{BET} (m ² /g)	448	439	496	493	635	676	924	788	572	1117
S_{meso} (m ² /g)	299	297	320	317	470	529	696	522	410	330
V_{pore} (cm ³ /g)	0.69	0.68	0.72	0.71	0.92	1.004	1.29	1.07	0.79	0.47
V_{meso} (cm ³ /g)	0.62	0.62	0.65	0.64	0.85	0.942	1.2	0.96	0.72	0.37
Pore size (Å)	129	127	129	130	112	90	100	113	130	22

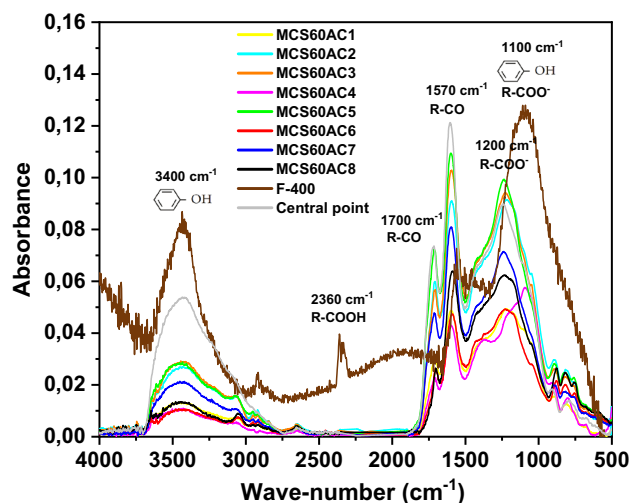


Fig. 2 FT-IR spectra for the synthesized activated carbons and commercial activated carbon F-400

mostly obtained during the activation step. Those oxygenated groups are relevant in the cation adsorption process due to their negative charge density [26]. The band at 3400 cm^{-1} is assigned to the O–H stretching corresponding to the OH^- ions in phenolic groups [27]. The band at 1700 cm^{-1} suggests the presence of $\text{C}=\text{O}$ groups, in ketones, aldehydes, carboxylic and benzenic acids [28]. The band around 1570 cm^{-1} is attributed to the $\text{C}=\text{O}$ stretching groups in lactones and carboxylic acids [29]. Finally, the peaks located between 1100 and 1200 cm^{-1} are widely associated to the CO and OH groups in phenolic and alcohol groups [30]. Having examined all the functional groups presented in the carbons, it can be noticed that the surface of the materials showed principally carboxyl and phenolic groups. The phenolic groups can help to decrease the pH (acidify the aqueous solution) by giving H^+ to the system for its dissociation, acting like a Brønsted acid with a pK_a value near 10 [31]. That behavior will prevent the cobalt precipitation phenomenon.

It can be appreciated that the mesoporous carbon synthesized in the fifth experiment ($-1-1+1$) shows the higher intensity in all previously mentioned peaks. As it will be indicated afterwards, this carbon is one which shows higher cobalt adsorption capacity. The activated carbon synthesized with the standard conditions showed the highest band intensity at 3400 cm^{-1} and 1570 cm^{-1} , proving the existence of a great deal of phenolic and carboxyl groups. For the F-400 carbon, the most important groups are located at 3400 and 1100 cm^{-1} ($\text{C}=\text{O}$ and $\text{O}-\text{H}$ groups), along with a small peak at 2360 cm^{-1} that can be linked to the presence of $\text{O}-\text{H}$ stretching groups of carboxylic groups. Since in the F-400 spectra, the height of the peaks is very similar, it can be concluded that the surface of this carbon is chemically heterogeneous. It shows many functional groups with no predominance whatsoever.

Experimental Design Results

The synthesis of mesoporous activated carbons involves the control of several variables such as the carbon source, the template, the thermal treatment, the particle size, among many others. In the present work, the last step of the synthesis, the activation process, key to obtain a carbon with good adsorption properties, was studied. The three existing variables, flow, temperature, and time will affect the activation yield since it is a controlled oxidation thermolytic process. By controlling these parameters the optimization of the process is achievable [17]. Table 4 displays the cobalt adsorption results with all the carbons and the orthogonal view of the results is displayed in Appendix A (electronic supplementary material). The most remarkable results can be found with the activated carbons seized with experiments 5 ($-1-1+1$) and 7 ($-1+1+1$), operating with low air flows and large activation times. The influence of these factors will be widely regarded hereinafter.

Once the results of the adsorption experiments were gathered, the A, B and C effects, the two-factor interaction effects, AB, AC, BC and the three-factor interaction effect, ABC, are estimated easily with linear combination, as well

Table 4 Results of the experimental design

Run	Coded factors			Cobalt removal (%)		
	A	B	C	Replicate 1	Replicate 2	Total
1	-1	-1	-1	33	37	(1)=0.69
2	+1	-1	-1	35	38	a=0.72
3	-1	+1	-1	27	29	b=0.56
4	+1	+1	-1	28	27	ab=0.55
5	-1	-1	+1	62	63	c=1.24
6	+1	-1	+1	18	23	ac=0.42
7	-1	+1	+1	61	61	bc=1.22
8	+1	+1	+1	7	3	abc=0.1

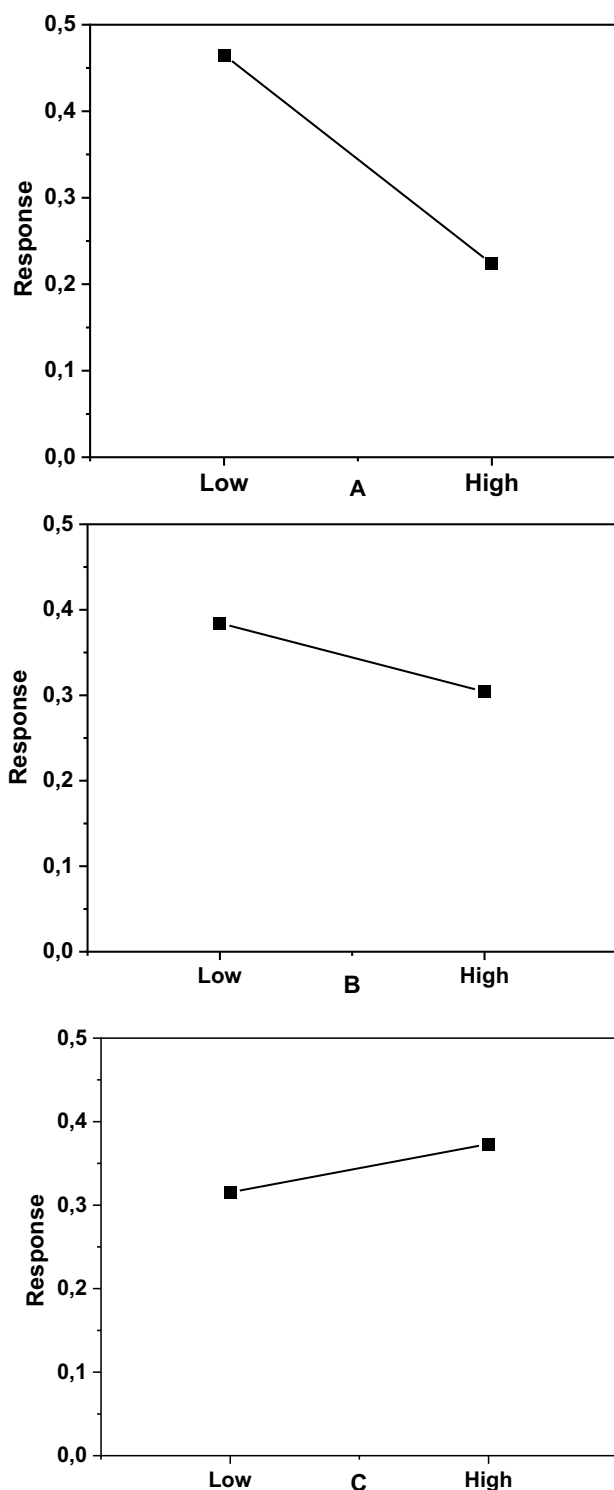
Table 5 Effects estimates, interactions, and sums of squares for the 2^3 factorial design

Factor	Contrast	Effect	Sum of Squares	Percent contribution (%)
A	- 1.9322	- 0.2415	0.2333	44.44
B	- 0.6414	- 0.0802	0.0257	4.90
C	0.4627	0.0578	0.0134	2.55
AB	- 0.3337	- 0.0417	0.0070	1.33
BC	- 0.0304	- 0.0038	0.0001	0.01
AC	- 1.9664	- 0.2458	0.2417	46.03
ABC	- 0.2504	- 0.0313	0.0039	0.75

as the contrasts and sum of squares calculation. The complete calculation process can be found in Appendix B (electronic supplementary material).

Table 5 summarizes the contrasts, effects, and sum of squares for the main factors and interactions in the factorial design. The column referred as percent contribution measures the contribution of each term to the total sum of squares. The factor that dominates the process was A, the air flow, considering that its effect was nearly ten times higher than B and C effects. This consideration also affects to the interactions, being AC the most influential to the response. The air flow had a great influence together with the activation time, and vice versa. The other factors and interactions have significantly less impact in the process. An ANOVA hypothesis test was carried out to verify whether the calculated effects are significant or not. The details of the ANOVA can be found in the Appendix C (electronic supplementary material). The development of the regression and model calculation can be found in Appendix D (electronic supplementary material).

Finally, the main effects of the factors A, B and C, in conjunction with the two-factor interactions are plotted in Figs. 3 and 4. As it was established in preliminary analysis, operating at the lower level for the temperature and for the air flow are positive to maximize the cobalt removal and the adsorption properties. On a physicochemical level, since the activation is a controlled oxidation thermolytic process, working at mild conditions leads to a lesser amount of burned carbon, improving properties such as the surface area. Thus, energy savings can be achieved as well. Regarding the activation time, working for 3 h returns a better output since, as it was discussed in the characterization section, in the experiments 5–8 the surface areas obtained are greater than the ones obtained with only 1 h of activation. The three main effect graphs have the same scale. Hence, the A factor (air flow) is the one with the highest importance, because of the steep slope. Comparing the FTIR of the samples activated with the flow in the higher level with those activated with the lowest flow (when the rest of variables

**Fig. 3** Individual factor graphs for the 2^3 factorial design. A factor effect (a), B factor effect (b), C factor effect (c)

are the same), it can be observed in Fig. 2 that reducing the flow in most cases led to an increase in the intensity of the bands, proving that an uncontrolled flow can negatively alter the surface chemical structure.

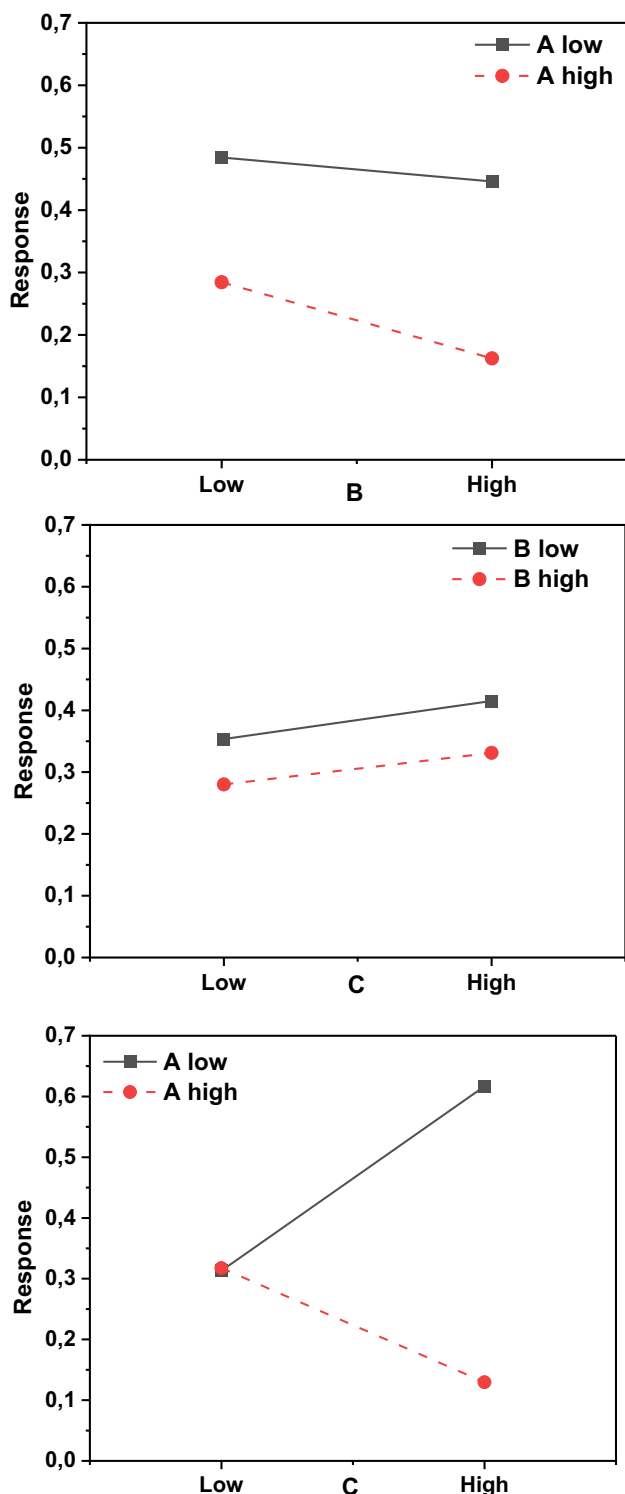


Fig. 4 Two-factor interaction graphs for the 2³ factorial design. AB interaction (a), BC interaction (b), AC interaction (c)

Some worthwhile conclusions can be drawn from the interaction graphs. When the lines are not parallel and/or intersect, the interaction is significant [23]. Thereby, AB

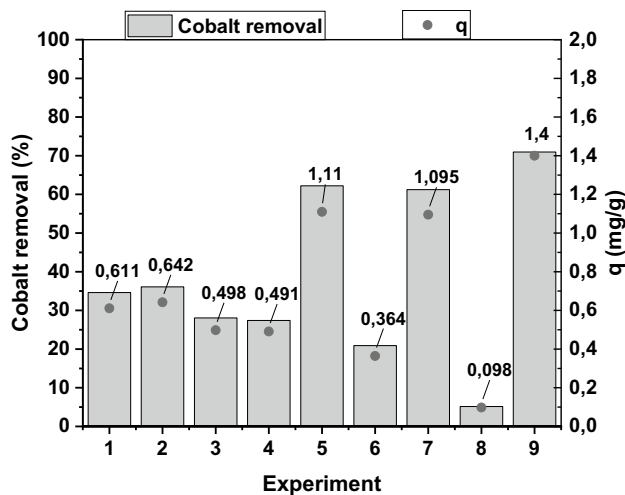


Fig. 5 Results of the cobalt adsorption tests for each experiment and the central point replication (exp. 9). Conditions: [Co²⁺]=20 mg/L, T=25 °C, speed = 1100 rpm, adsorbent dosage = 10 g/L

interaction is considerably low, especially when A is in the low level. Working in the higher level of A increases the interaction, and the temperature becomes an important factor in the process. Basically, at higher rates of air flow, increasing the temperature leads to an uncontrolled combustion, to the point of partially burning the carbon. BC interaction barely has relevance, no matter in which level the temperature is. Increasing the activation time slightly improves the response. Finally, AC interaction seems to be the key to the system. While working at the lower level of the air flow, an increase in the activation time improves the results. With this moderate flow, the thermal treatment applied to the carbon is far smoother, with a controlled improvement in the surface properties, for instance the presence of oxygenated groups such as COOH, O–H and C=O (see FTIR of experiments 3, 5 and central point in Fig. 2). With this combination, exemplified in the experiments 5 and 7, the best results can be achieved. On the other hand, while working with large air flow, the larger the time, the worse the results. In this case, the oxidation is totally uncontrolled through the process. While flow seemed to have a larger importance in the presence of functional groups, activation time (experiments 5–8) helped to increase the overall surface area of the carbons and, in inverse proportion, to decrease the pore size. Pore size that will be wide enough to achieve the fast adsorption of cobalt hydrated ions in any case.

Kinetic and Equilibrium Studies

The results for the adsorption experiments are displayed in the Fig. 5, including the experiment carried out with the central point conditions (experiment 9). Percentage of cobalt removal and adsorption capacity are shown. The average

value of the two adsorption experiments performed with each carbon ($n=2$) is shown. For all experiments, the final pH was ranging between 3 and 4, decreasing from the initial pH of the cobalt aqueous solutions (around 5–6), because of the acidic character of the activated carbons. This guaranteed that precipitation was not occurring, since cobalt tends to precipitate when pH exceeds 8. The experiments 5 and 7 showed the highest adsorption capacities, set in 1.1 mg/g. The experiment 9, the central point (0 0 0) reached the highest adsorption results. That performance can be accounted for the large number of oxygenated surface groups, according to the intensity of the bands in Fig. 2. The activation process in those intermediate conditions achieved great properties, without an excessive burning of the carbon. The great deal of phenolic and carboxyl groups, especially the first ones, provide an important negative charge density, for the acidic character of that groups and the delocalized electron present in the benzene rings. As it was established in the experimental design, the activation using moderate air flows leads to a further development of the surface chemistry of these mesoporous carbons, with a considerable rise in the intensity of the absorption bands obtained in the FTIR analysis. More importantly, this balance between moderate air flows and large activation times can reach an equilibrium among the textural and chemistry properties of the activated carbon, conditions perfectly condensed in the carbon with the central point conditions. Therefore, the kinetic and equilibrium studies will be performed with that carbon. Not only that, but a comparison with a microporous carbon, commercial F-400 will be carried out [31], in order to determine how important the mesoporosity is to achieve faster adsorption kinetics.

Kinetic curves, represented in Fig. 6, showed that the removal of cobalt was considerably faster using the mesoporous carbon than using the microporous F-400. With the mesoporous material, the equilibrium was reached within the first 15 min (represented in the zoomed area), removing the 67% of the initial cobalt, with an adsorption capacity of 1.7 mg/g. By contrast, the adsorption onto the F-400 carbon was slower, needing 24 h to reach equilibrium. At that point, the 77% of initial cobalt was removed, being 1.7 mg/g the adsorption capacity. The differences reside mainly in the porosity of each material. According to Table 3, F-400 has a pore size distribution centered in 20 Å, in the micropore range. On the other hand, the mesoporosity is notable for the synthesized activated carbon, having a 72% of mesoporous surface and a pore size distribution centered in 130 Å. This size is larger than the diameter of the hydration cobalt solvation shell ($[\text{Co}(\text{H}_2\text{O})_6]^{2+}$) which is 8.46 Å [32]. Observing the FTIR spectrum, since the adsorption rates are similar, the remarkable presence of phenolic (F-400) and carbonyl/carboxyl (mesoporous carbon) groups have their importance in the cobalt adsorption process by electrostatic interactions.

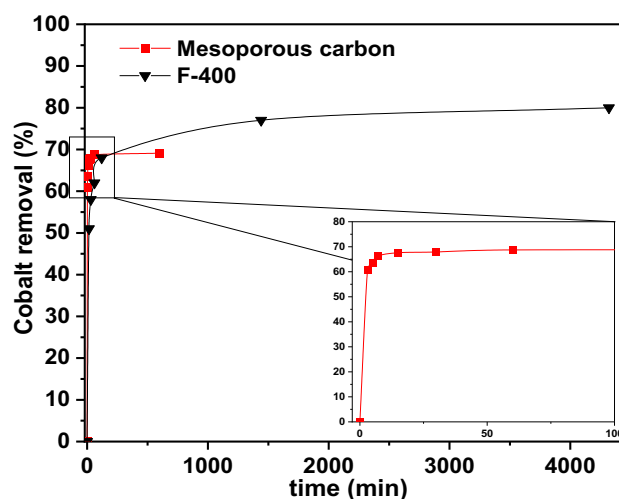


Fig. 6 Cobalt adsorption kinetics onto F-400 and mesoporous activated carbon. Conditions: $[\text{Co}^{2+}] = 20$ mg/L, $T = 25^\circ\text{C}$, speed = 1100 rpm, adsorbent dosage = 10 g/L, particle size = powder < 500 μm

Regarding the adsorption mechanism, it has four consecutive mass transfer steps: external diffusion, film diffusion, internal transport through the pore structure and adsorption [33]. Since the average pore size 15 times higher than the hydrated diameter of cobalt, internal diffusion resistance is expected to be negligible using mesoporous carbon, so the kinetics are faster. With the F-400 carbon, even though the average pore size is higher than the cobalt diameter, it might appear some steric hindrance, that can slow down the process. Therefore, more contact time is required to reach equilibrium.

To elucidate the adsorption mechanism, the experimental kinetics obtained were adjusted to three different kinetic models, such as the pseudo-first order (Eq. (3)), the pseudo-second order (Eq. (4)), Elovich (Eq. (5)) and the diffusion model Weber-Morris (Eq. (6)). Pseudo-first order model identifies adsorption as a chemical reaction, where the rate constant k_1 (min^{-1}) is not concentration dependent. Pseudo-second order model states that the overall process is controlled by the proper adsorption step, and it does not depend on mass transfer resistance; k_2 ($\text{g}/\text{min mg}$) represents the second order rate constant [34]. Elovich model is applied to adsorption onto energetically heterogeneous surfaces. For this model, v_0 is the initial adsorption rate ($\text{g}/\text{mg}\cdot\text{min}$) and β (g/mg) is related to the surface coverage and activation energy [35]. Weber-Morris model tries to identify the diffusion mechanism during the process. It establishes if there is intraparticle or boundary layer diffusion. C is the intersection to the ordinate axis and k_i ($\text{mg}/\text{g}\cdot\text{min}^{1/2}$) is the intraparticle diffusion rate constant [36]. q_e and q represent the adsorption capacities at equilibrium and at t time, respectively (mg/g). The fitted data graphs for the four models studied is represented in Appendix E (electronic supplementary material).

Table 6 summarizes the parameters for the kinetic models, while Table 7 shows the parameters for the Weber–Morris model.

$$\text{Ln}(q_e - q) = \text{Ln}(q_e) - k_1 \cdot t \tag{3}$$

$$\frac{t}{q} = \frac{1}{k_2 q_e^2} + \frac{1}{q_e} t \tag{4}$$

$$q = \frac{1}{\beta} \cdot \text{Ln}(v_0 \cdot \beta) + \frac{1}{\beta} \cdot \text{Ln}(t) \tag{5}$$

$$q = k_i \cdot t^{\frac{1}{2}} + C \tag{6}$$

As expressed in Table 6, pseudo-second order model fits better (higher R^2 value) for both mesoporous and F-400 adsorption of cobalt. Thus, due to adsorption process is controlled by the adsorption step, the external and internal mass transfer resistances do not affect the overall process. This conclusion agreed with the previously discussed results since pore size is enough to allow complete mobility of the hydrated molecules through the internal structure of the solid. It can be asserted that, since the controlling mechanism for the mesoporous materials is not the internal diffusion, the textural changes observed in the different activation conditions will not substantially affect the adsorption process. Instead, the variation in the

surface chemistry gains importance for the adsorptive performance. It is also interesting to appreciate how well the Elovich model fits the data from the F-400 adsorption, in contrast to the poor adjustment to the mesoporous data. As it was affirmed in the FTIR analysis, the surface of the F-400 carbon has a marked heterogeneity, while the surface of the mesoporous carbon is mainly constituted by carboxyl and phenolic groups. The Weber–Morris model applied to the F-400 experimental data does cross the coordinate origin, so the intraparticle diffusion can affect the adsorption process. Nonetheless the fit is worse than the previously obtained with the pseudo-second order and the Elovich models.

To elucidate the nature of the adsorption interactions, the enthalpy in the cobalt-mesoporous carbon adsorption was calculated by carrying out kinetic experiments at 25 °C, 35 °C and 45 °C. In these experiments it was observed that adsorption capacity only varied a 6% amongst experiments, it was almost constant (see Table 8). From these values, the equilibrium constant was calculated with Eq. (7), Gibbs free energy (ΔG° (kJ/mol)) was determined with Eq. (8), and standard enthalpy (ΔH° (kJ/mol)) and entropy (ΔS° (J/mol K)) were calculated applying the Van't Hoff equation, Eq. (10). In these equations, C_0 and C_e are the initial and equilibrium cobalt concentration (mg/L), and R represents the universal gas constant (8.134 J/mol K).

Table 6 Kinetic fitting parameters for F-400 and mesoporous activated carbon

Adsorbent	Pseudo-first order			Pseudo-second order			Elovich		
	q_e	k_1	R^2	q_e	k_2	R^2	v_0	β	R^2
	mg/g	min ⁻¹		mg/g	g/mg·min		g·mg/min	g/mg	
F-400	0.617	0.001	0.919	1.725	0.024	0.999	144.13	8.89	0.989
Mesoporous carbon	0.091	0.001	0.693	1.713	2.357	0.999	1.22·10 ²⁸	43.29	0.515

Table 7 Diffusion model fitting parameters for F-400 and mesoporous activated carbon

Adsorbent	First section			Second section		
	k_i	C	R^2	k_i	C	R^2
	mg/g·min ^{1/2}	mg/g		mg/g·min ^{1/2}	mg/g	
F-400	0.172	0.152	0.879	0.006	1.362	0.932
Mesoporous carbon	0.444	0.367	0.744	7.95E–04	1.685	0.137

Table 8 Thermodynamic analysis of the cobalt adsorption onto mesoporous carbon

T (K)	q_{eq} (mg/g)	K_C	ΔG° (kJ/mol)	R^2	ΔH° (kJ/mol)	ΔS° (J/molK)
298	1.713	1.95	-1.65		-4.73	-10.31
308	1.611	1.82	-1.53	0.99		
318	1.562	1.73	-1.45			

$$K_C = \frac{C_0 - C_e}{C_e} \tag{7}$$

$$\Delta G^\circ = -R \cdot T \cdot \ln K_C \tag{8}$$

$$\Delta G^\circ = \Delta H^\circ - T \cdot \Delta S^\circ \tag{9}$$

$$-\ln(K_C) = \left(\frac{\Delta H^\circ}{R} \right) \cdot \frac{1}{T} - \frac{\Delta S^\circ}{R} \tag{10}$$

Table 8 shows the results for the thermodynamic analysis. Since ΔG° and ΔH° values are below zero, this can be stated as an exothermic process. Standard enthalpy value, -4.73 kJ/mol, is lower than the minimum value for chemisorption, which is -50 kJ/mol [33]. Standard Gibbs free energy value, -1.65 kJ/mol, falls inside the range between 0 and -20 kJ/mol, again a measure of physisorption [37]. Adsorption onto the mesoporous activated carbon is ruled by the weak van der Waals forces, induction, dispersion, and dipole–dipole interactions. ΔS° below zero indicates a decrease in the disorder degree of the system, caused by the immobilization of the Co^{2+} ions in the adsorbent

surface. The plot of Van't Hoff equation is displayed in Appendix F (electronic supplementary material).

The determination of the equilibrium mechanism or the mesoporous carbon (equilibrium isotherm) is shown in the Fig. 7. Langmuir isotherm (Eq. (11)) suggests adsorption in monolayer, in energetically homogeneous surfaces. The molecules are sorbed in well-defined sorption sites. In this model, b_L (L/mg) represents the affinity between adsorbate and adsorbent. Freundlich isotherm (Eq. (12)) applies to energetically heterogeneous systems, with a varied surface chemistry. In this model, k_F (L/mg) is the adsorption coefficient, representing the adsorbate adhesion onto the surface and $1/n$ is related to the heterogeneity of the adsorbent surface. Sips isotherm (Eq. (13)) develops the Langmuir model with three parameters. It adds the n parameter to evaluate the heterogeneity of the surface. In these expressions, q_e y q_{sat} represent the adsorption capacities at equilibrium and the maximum capacity of adsorption, respectively (mg/g). C_e is the cobalt concentration in the equilibrium (mg/L) [38].

$$q_e = \frac{q_{\text{sat}} \cdot b_L \cdot C_e}{1 + b_L \cdot C_e} \tag{11}$$

$$q_e = k_F \cdot C_e^{1/n_F} \tag{12}$$

$$q_e = \frac{q_{\text{sat}} \cdot b_s \cdot C_e^{1/n}}{1 + b_s \cdot C_e^{1/n}} \tag{13}$$

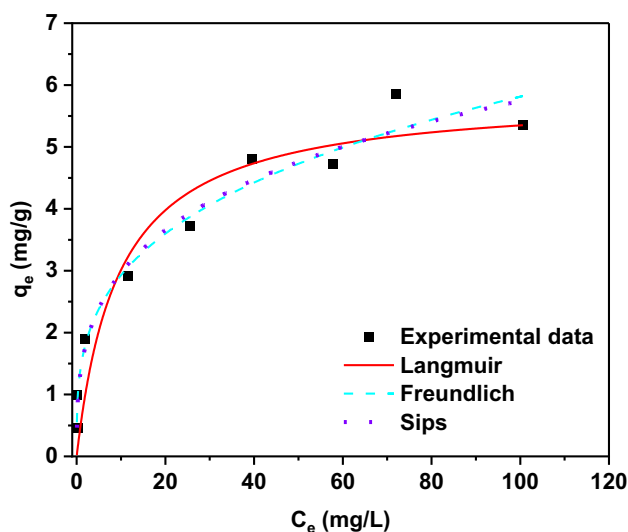


Fig. 7 Cobalt adsorption isotherms onto mesoporous activated carbon. Conditions: $T=25^\circ\text{C}$, speed = 1100 rpm, carbon dosage = 10 g/L

As it can be seen in Table 9, Freundlich and Sips models properly fit the experimental data for the mesoporous adsorption isotherm. Both models are suitable to describe adsorption in multilayer, and a predominant heterogeneous and disordered surface. Plus, according to the Sips model, the value of $n=2.83$ obtained during the fitting supports the idea of a heterogeneous surface, since this value is close to 1 in homogeneous surfaces (Langmuir equation). The saturation of this carbon occurs at 5.8 mg Co^{2+} /g carbon.

Finally, Table 10 overviews the advantages of using mesoporous activated carbons in terms of kinetics and cobalt removal efficiency, as a comparison with other microporous and mesoporous materials found in literature.

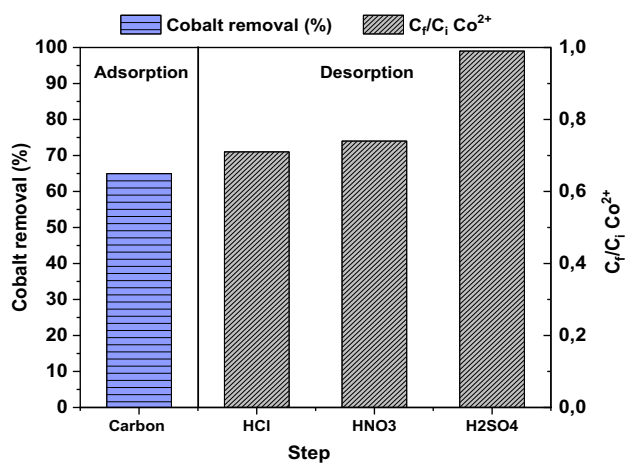
The main benefits of using mesoporous activated carbons are highlighted in Table 10, mostly the ultra-fast kinetics reached, and the optimal cobalt removal achieved, very

Table 9 Isotherm fitting parameters for mesoporous activated carbon

Adsorbent	Langmuir			Freundlich			Sips			
	q_{sat}	b_L	R^2	k_F	n_F	R^2	q_{sat}	b_S	n	R^2
	mg/g	L/mg		L/mg			mg/g	L/mg		
Mesoporous carbon	5.85	0.11	0.91	1.47	3.36	0.96	22.68	0.07	2.83	0.96

Table 10 Cobalt removal capacities and kinetics of different adsorbents

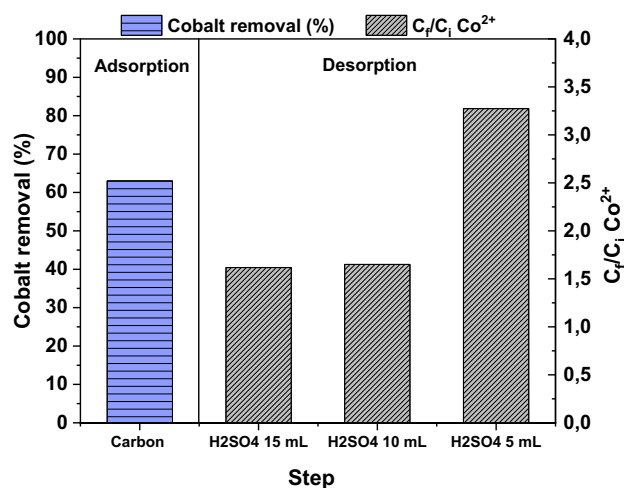
Adsorbent	q_{\max} (mg/g)	Equilibrium time (min)	Reference
Ordered mesoporous carbon (CMK-3)	5.4	100	[21]
Ordered mesoporous carbon (PCK)	1.6	6	[22]
Dolomite	2.8	120	[39]
Microporous F400 activated carbon	3	5760	[28]
Microporous 13X zeolite	4	240	[40]
Disordered mesoporous carbon	5.8	15	This work

**Fig. 8** Cobalt adsorption results onto mesoporous activated carbon and cobalt desorption using different acids. Conditions: $[\text{Co}^{2+}] = 20 \text{ mg/L}$, $T = 25 \text{ }^\circ\text{C}$, speed = 650 rpm, carbon dosage = 10 g/L, acid volume = 20 mL, acid pH 2.5

similar to other materials such as zeolites and natural sorbents, with the advantages of lesser contact times and the energy savings associated with it.

Desorption Experiments

With the aim of recovering the adsorbed metal and performing an integral treatment to the polluted water, a final acid desorption study was performed, with HCl, HNO₃ and H₂SO₄ as alternatives. Acid pH was adjusted to 2.5. Figure 8 presents the results of the desorption test, performed right after an adsorption trial with the mesoporous activated carbon. The desorption rate was calculated as final concentration/adsorbed concentration. The adsorption tests were performed in triplicate (overall Co²⁺ removal = 65%), so after that each point was put in contact with each acid. H₂SO₄ was the best performing acid, recovering almost the 100% of the adsorbed acid from the carbon. HCl and HNO₃ only achieved 71% and 74% recovery degrees, respectively. The desorption process can be explained for the decrease in the pH of the media, which makes the surface of the adsorbent more and more

**Fig. 9** Cobalt adsorption results onto mesoporous activated carbon and cobalt reconcentration using H₂SO₄. Conditions: $[\text{Co}^{2+}] = 20 \text{ mg/L}$, $T = 25 \text{ }^\circ\text{C}$, speed = 650 rpm, carbon dosage = 10 g/L, acid volume = 5, 10 and 15 mL, acid pH 2.5

positive. Therefore, the electrostatic repulsion for the growing existence of free H⁺ ions in the system increases, so the cations are removed from the surface [41].

Once evaluated the potential of sulfuric acid for cobalt desorption, a pre-concentration experiment was executed. The previous experiment was repeated, but only using H₂SO₄ in a lower volume: 15, 10 and 5 mL. Figure 9 exemplifies the adsorption and reconcentration results. By reducing the acid volume to 15 or 10 mL, the cobalt was reconcentrated to the 165% of the adsorbed cobalt concentration (from 12 to 20 mg/L). By employing only 5 mL of H₂SO₄ the reconcentration was even amplified, and a 38 mg/L cobalt solution was obtained. That represents a concentration of 325% from the adsorbed cobalt concentration and a 190% from the initial cobalt solution (20 mg/L).

It can be concluded that this acid is efficient both for cobalt desorption and pre-concentration. This pre-concentration allows to explore the possibility of reusing this recovered cobalt as secondary raw material source in future studies.

Recycling of the Mesoporous Material

To approach the circular economy concept, the recycling of the activated mesoporous carbon should be studied. The regeneration of the carbon is one of the main advantages of the adsorption technology [33]. Hence, once stated in the previous section that acid desorption with sulfuric acid is highly efficient to release the adsorbed cations, a subsequent experiment was conducted. After the desorption step with H₂SO₄ (pH 2.5), the *x*% of adsorbed Co²⁺ ions were recovered from the material. The unloaded carbon was washed with deionized water, then dried in the oven overnight. Another adsorption experiment was executed, with the exact same conditions than the performed throughout the work (dosage = 10 g/L, [Co²⁺] = 20 mg/L, T = 25 °C). The recycled and regenerated carbon showed only a 5% of loss of adsorption capacity, stating that it could be reused effectively. This can positively affect the economy of the process.

Conclusions

The optimization of the activation step in the mesoporous activated carbon synthesis has been carried out. It has been observed that air flow is the predominant factor, achieving better cobalt adsorption results working in the lower level of this variable. Temperature and time showed a slightly lower influence in the process, being the optimal point working at low temperatures and large times. The interactions between all the factors have been proven as significant, except for the temperature—time interaction. Air flow—time interaction had a 46% effect in the response, being the optimal point at low flows and large times. Working at extended times helped to increase the surface area of the carbons, and moderated air flows developed a greater number of oxygenated groups for cobalt adsorption. Kinetic studies demonstrated that activated mesoporous carbon enabled quick kinetics, reaching the equilibrium up to 99% faster than using a microporous F-400 activated carbon, only in 15 min the 66% of initial Co²⁺ was removed. The obtained kinetics were fitted to a pseudo-second order model, so the adsorption step ruled the process. The equilibrium study proved that the maximum adsorption capacity was found in 5.8 mg/g. The experimental data showed an excellent fit to the Freundlich and Sips models, stating that there was a multilayer heterogeneous adsorption process. Desorption studies demonstrated the feasibility of desorbing the adsorbed cobalt using sulfuric acid, and the pre-concentration of the desorbed cobalt was performed, up to 2 times the initial concentration value, by reducing the volume to the quarter.

Supplementary Information The online version contains supplementary material available at <https://doi.org/10.1007/s40831-022-00644-3>.

Acknowledgements This work was supported by the financial support of the Santander-UCM 2018 project (PR75718) and by the contract of research assistant from the Community of Madrid through the program “Garantía Juvenil” [PEJ-2020-AI/IND-17675]. The authors also thank the Correlation Spectroscopy Research Centre of the Complutense University of Madrid for helping with the characterization.

Funding Open Access funding provided thanks to the CRUE-CSIC agreement with Springer Nature.

Data Availability Data will be available on request.

Declarations

Conflict of interest The authors declare that they have no conflicts of interest.

Informed consent Informed consent was obtained from all individual participants included in the study.

Research involving animal rights This article does not contain any studies with animals performed by any of the authors.

Open Access This article is licensed under a Creative Commons Attribution 4.0 International License, which permits use, sharing, adaptation, distribution and reproduction in any medium or format, as long as you give appropriate credit to the original author(s) and the source, provide a link to the Creative Commons licence, and indicate if changes were made. The images or other third party material in this article are included in the article's Creative Commons licence, unless indicated otherwise in a credit line to the material. If material is not included in the article's Creative Commons licence and your intended use is not permitted by statutory regulation or exceeds the permitted use, you will need to obtain permission directly from the copyright holder. To view a copy of this licence, visit <http://creativecommons.org/licenses/by/4.0/>.

References

1. Eddy M (2001) Ingeniería de aguas residuales. McGraw-Hill, New York
2. Brutland (1987) Report of the World Commission on Environment and Development
3. Endo A, Tsurita I, Burnett K, Orenco PM (2017) A review of the current state of research on the water, energy, and food nexus. *J Hydrol* 11:20–30. <https://doi.org/10.1016/j.ejrh.2015.11.010>
4. Barakat MA (2011) New trends in removing heavy metals from industrial wastewater. *Arab J Chem* 4:361–377. <https://doi.org/10.1016/j.arabjc.2010.07.019>
5. Kurniawan TA, Chan GYS, Lo W-H, Babel S (2006) Physico-chemical treatment techniques for wastewater laden with heavy metals. *Chem Eng J* 118:83–98. <https://doi.org/10.1016/j.cej.2006.01.015>
6. Programme UNE, Panel IR (2011) Recycling rates of metals: a status report
7. International Energy Agency (2021) The role of critical minerals in clean energy transitions. World Energy Outlook Special Report
8. Patricia AD, Darina B, Claudiu P, Nikolaos A (2018) Cobalt: demand-supply balances in the transition to electric mobility

9. Scheele F, de Haan E, Kiezebrink V (2016) Cobalt blues environmental pollution and human rights violations in Katanga's copper and cobalt mines. SOMO. <https://www.somo.nl/cobalt-blues/>
10. Botelho Junior AB, Stopic S, Friedrich B et al (2021) Cobalt recovery from Li-ion battery recycling: a critical review. *Metals* 11:1999. <https://doi.org/10.3390/met11121999>
11. Swain B (2017) Recovery and recycling of lithium: a review. *Sep Purif Technol* 172:388–403. <https://doi.org/10.1016/j.seppur.2016.08.031>
12. Gunatilake S (2015) Methods of removing heavy metals from industrial wastewater. *J Multidiscipl Eng Sci Stud* 1:12–18
13. Budnyak TM, Piątek J, Pylypchuk IV et al (2020) Membrane-filtered kraft lignin-silica hybrids as bio-based sorbents for cobalt(II) ion recycling. *ACS Omega* 5:10847–10856. <https://doi.org/10.1021/acsomega.0c00492>
14. Liu Y, Liu Y, Tang L et al (2019) Chapter 3—Mesoporous carbon-based composites for adsorption of heavy metals. In: Tang L, Deng Y, Wang J et al (eds) *Nanohybrid and nanoporous materials for aquatic pollution control*. Elsevier, Amsterdam, pp 63–102
15. Díez E, Gómez JM, Rodríguez A et al (2020) A new mesoporous activated carbon as potential adsorbent for effective indium removal from aqueous solutions. *Microporous Mesoporous Mater* 295:109984. <https://doi.org/10.1016/j.micromeso.2019.109984>
16. Galán J, Rodríguez A, Gómez JM et al (2013) Reactive dye adsorption onto a novel mesoporous carbon. *Chem Eng J* 219:62–68. <https://doi.org/10.1016/j.cej.2012.12.073>
17. Kyotani T (2000) Control of pore structure in carbon. *Carbon* 38(2):269–286. [https://doi.org/10.1016/S0008-6223\(99\)00142-6](https://doi.org/10.1016/S0008-6223(99)00142-6)
18. Lu A-H, Zhao D (2009) *Nanocasting: a versatile strategy for creating nanostructured porous materials*. RSC Publishing, Cambridge
19. Stathi P, Dimos K, Karakassides MA, Deligiannakis Y (2010) Mechanism of heavy metal uptake by a hybrid MCM-41 material: surface complexation and EPR spectroscopic study. *J Colloid Interface Sci* 343:374–380. <https://doi.org/10.1016/j.jcis.2009.11.029>
20. Barczak M, Michalak-Zwierz K, Gdula K et al (2015) Ordered mesoporous carbons as effective sorbents for removal of heavy metal ions. *Microporous Mesoporous Mater* 211:162–173. <https://doi.org/10.1016/j.micromeso.2015.03.010>
21. Boumessaïdia S, Cheknane B, Bouchenafa-Saïb N et al (2019) Elimination of cobalt (II) by adsorption on mesoporous materials and carbons of types SBA-15, CMI-1. *Alger J Environ Sci Technol* 5:1046–1054
22. Siddiqui MN, Chanbasha B, Al-Arfaj AA et al (2021) Superfast removal of cobalt metal ions in water using inexpensive mesoporous carbon obtained from industrial waste material. *Environ Technol Innov*. <https://doi.org/10.1016/j.eti.2020.101257>
23. Montgomery DC (2008) *Design and analysis of experiments*. Wiley, New York
24. Krishnan A, Anirudhan T (2008) Kinetic and equilibrium modelling of cobalt(II) adsorption onto bagasse pith based sulphurised activated carbon. *Chem Eng J* 137:257–264. <https://doi.org/10.1016/j.cej.2007.04.029>
25. Thommes M, Kaneko K, Neimark AV et al (2015) Physisorption of gases, with special reference to the evaluation of surface area and pore size distribution (IUPAC Technical Report). *Pure Appl Chem* 87:1051–1069. <https://doi.org/10.1515/pac-2014-1117>
26. Wu Z, Webley PA, Zhao D (2010) Comprehensive study of pore evolution, mesostructural stability, and simultaneous surface functionalization of ordered mesoporous carbon (FDU-15) by wet oxidation as a promising adsorbent. *Langmuir* 26:10277–10286. <https://doi.org/10.1021/la100455w>
27. Hadoun H, Sadaoui Z, Souami N et al (2013) Characterization of mesoporous carbon prepared from date stems by H₃PO₄ chemical activation. *Appl Surf Sci* 280:1–7. <https://doi.org/10.1016/j.apsusc.2013.04.054>
28. Gómez JM, Díez E, Bernabé I et al (2018) Effective adsorptive removal of cobalt using mesoporous carbons synthesized by silica gel replica method. *Environ Process* 5:225–242. <https://doi.org/10.1007/s40710-018-0304-9>
29. Pretsch E, Buhlmann P, Badertscher M (2009) *Structure determination of organic compounds*. Springer-Verlag, Berlin, pp 1–88
30. Hesse M (2005) *Métodos espectroscópicos en química orgánica*, 2^a ed. act. y amp. Síntesis, Madrid
31. Galán del Álamo J (2013) *Preparación y síntesis de materiales adsorbentes para la eliminación de contaminantes en efluentes acuosos*. Info:eu-repo/semantics/doctoralThesis, Universidad Complutense de Madrid
32. Pavel CC, Vuono D, Asaftei IV et al (2005) Study of the thermal dehydration of metal-exchange ETS-10 titanosilicate. In: Čejka J, Žilková N, Nachtigall P (eds) *Studies in surface science and catalysis*. Elsevier, Amsterdam, pp 805–812
33. Worch E (2012) *Adsorption technology in water treatment: fundamentals, processes, and modeling*. Walter de Gruyter, Berlin
34. Simonin J-P (2016) On the comparison of pseudo-first order and pseudo-second order rate laws in the modeling of adsorption kinetics. *Chem Eng J* 300:254–263. <https://doi.org/10.1016/j.cej.2016.04.079>
35. Aharoni C, Tompkins FC (1970) Kinetics of adsorption and desorption and the Elovich equation. In: Eley DD, Pines H, Weisz PB (eds) *Advances in catalysis*. Academic Press, New York, pp 1–49
36. Weber WJ, Morris JC (1963) Kinetics of adsorption on carbon from solution. *J Sanit Eng Div* 89:31–59. <https://doi.org/10.1061/JSEDAI.0000430>
37. Yu F, Wu Y, Li X (2012) Kinetic and thermodynamic studies of toluene, ethylbenzene, and m-xylene adsorption from aqueous solutions onto KOH-activated multiwalled carbon nanotubes. *J Agric Food Chem*. <https://doi.org/10.1021/jf304104z>
38. Saadi R, Saadi Z, Fazaeli R, Fard N (2015) Monolayer and multilayer adsorption isotherm models for sorption from aqueous media. *Korean J Chem Eng*. <https://doi.org/10.1007/s11814-015-0053-7>
39. Ghaemi A, Torab-Mostaedi M, Shahhosseini S, Asadollahzadeh M (2013) Characterization of Ag(I), Co(II) and Cu(II) removal process from aqueous solutions using dolomite powder. *Korean J Chem Eng* 30:172–180. <https://doi.org/10.1007/s11814-012-0113-1>
40. Jin Y, Wu Y, Cao J, Wu Y (2015) Adsorption behavior of Cr(VI), Ni(II), and Co(II) onto zeolite 13x. *Desalin Water Treat* 54:511–524. <https://doi.org/10.1080/19443994.2014.883333>
41. Yuan S, Xi Z, Jiang Y et al (2007) Desorption of copper and cadmium from soils enhanced by organic acids. *Chemosphere* 68:1289–1297. <https://doi.org/10.1016/j.chemosphere.2007.01.046>

Publisher's Note Springer Nature remains neutral with regard to jurisdictional claims in published maps and institutional affiliations.